OPEN ACCESS

Determining the Length Scale of Transport Impedances in Li-Ion Electrodes: Li(Ni$_{0.33}$Mn$_{0.33}$Co$_{0.33}$)O$_2$

View the article online for updates and enhancements.

Determining the Length Scale of Transport Impedances in Li-Ion Electrodes: Li(Ni$_{0.33}$Mn$_{0.33}$Co$_{0.33}$)O$_2$

Zeyu Hui,[1,2] Karthik S. Mayilvahanan,[1] Yuan Yang,[2] and Alan C. West[1,3,*,z]

[1]Department of Chemical Engineering, Columbia University, New York, New York 10027, United States of America
[2]Department of Applied Physics and Applied Mathematics, Columbia University, New York, New York 10027, United States of America
[3]Department of Earth and Environmental Engineering, Columbia University, New York, New York 10027, United States of America

Battery cathodes are complex multiscale, multifunctional materials. The length scale at which the dominant impedance arises may be difficult to determine even with the most advanced experimental characterization efforts, and thus modeling can play an important role in analysis. Discharge and voltage relaxation curves, interrogated with theory, are used to distinguish between transport impedance that arise on the scale of the active crystal and on the scale of agglomerates (secondary particles) comprised of nanoscale crystals. Model-selection algorithms are applied to determine that the agglomerate scale is dominant in the Li(Ni$_{0.33}$Mn$_{0.33}$Co$_{0.33}$)O$_2$ electrode studied here. Furthermore, conditions where the agglomerate and crystal-scale models yield distinct simulation results are demonstrated, providing approaches that can be applied to other systems.

List of symbols

Electrode Scale Symbols

a	Specific surface area (cm^{-1})
c_0	Concentration of lithium in the electrolyte (mol cm^{-3})
c_{bulk}	Concentration of lithium in the bulk electrolyte, 1×10^{-3} (mol cm^{-3}) in study.
$i_{applied}$	Applied current density (A cm^{-2})
D_0	Diffusion coefficient for lithium ions in bulk electrolyte, 1×10^{-6} (cm^2 s^{-1}).
$D_{0,eff}$	Effective electrolyte diffusion coefficient (cm^2 s^{-1})
$L_{cathode}$	Thickness of NMC cathode, 25 (μm) in experiment
$L_{separator}$	Thickness of separator, 25 (μm) in experiment
N_+	Flux of lithium ions in electrolyte (cm^{-2} s^{-1})
ϵ	Void fraction of porous electrode (porosity), 0.673 in experiment.
σ	Solid state conductivity (S cm^{-1})
κ	Solution conductivity (S cm^{-1})
z_i	Species charge
u_i	Species mobility (cm^2 s mol J^{-1})
Φ_1	Solid state potential (V)
Φ_2	Solution potential (V)

Crystal Scale Symbols

$c_s{}^x$	Concentration of lithium in NMC_{111} inside crystals (mol cm^{-3})
D_x	Diffusion coefficient for lithium in the NMC_{111} crystals
L_x	Average radius of NMC_{111} crystals, 200 (nm) in experiment

Agglomerate Scale Symbols

a^{agg}	Specific surface area inside agglomerate (cm^{-1})
A_{agg}	Average cross-sectional area of agglomerates (cm^2)
V_{agg}	Average volume of agglomerates (cm^3)
$c_0{}^{agg}$	Concentration of lithium in the electrolyte inside agglomerate (mol cm^{-3})
$c_s{}^{agg}$	Concentration of lithium in NMC_{111} inside agglomerate (mol cm^{-3})
D_{agg}	Diffusion coefficient for lithium ions in the NMC_{111} agglomerate (cm^2 s^{-1})
L_{agg}	Average radius of NMC_{111} agglomerates, 5 (nm) in experiment
$N_+{}^{agg}$	Flux of lithium ions in electrolyte inside agglomerate (cm^{-2} s^{-1})
ϵ^{agg}	Void fraction inside agglomerate
$\Phi_1{}^{agg}$	Solid state potential (V)
$\Phi_2{}^{agg}$	Solution potential (V)

Reaction Thermodynamics and Charge Transfer Kinetics Symbols

F	Faraday's constant (96,485 C mol^{-1})
k_{rxn}	Reaction rate constant for insertion of lithium inside NMC (cm$^{5/2}$ mol$^{-1/2}$ s^{-1})
i_{in}	Local current density for lithium insertion (A cm^{-2})
i_0	Exchange current density for lithium insertion (A cm^{-2})
R	Ideal gas constant (8.314 J mol^{-1} K^{-1})
T	Temperature, 298(K) in experiment
U	Reversible potential for lithium insertion reaction(V)
α_a	Anodic charge transfer coefficient, 0.5 in experiment
α_c	Cathodic charge transfer coefficient, 0.5 in experiment
η	Overpotential for lithium insertion reaction (V)

Lithium ion Batteries (LIBs) have garnered great research attention and wide commercial applications as energy storage devices on portable devices and electric vehicles (EV).[1,2] However, the optimization of LIBs for energy and power density is still an active research area.[3–6] For instance, compared with the graphite anodes (~372 mAh g^{-1} in specific capacity), cathode materials are lower in capacity (<250 mAh g^{-1}).[7] There are attempts to increase cathode mass loading (mass or capacity per area) by increasing cathode thickness or reducing porosity (roll pressing),[8] while others focus on increasing the upper limit of the voltage window, in order to gain more capacity from the cathode.[9] In both cases, transport of lithium and homogeneity of lithium intercalation/de-intercalation reaction may be crucial to battery performance.[10]

During battery operation, these processes occur at multiple length scales. Lithium ions inside liquid electrolyte diffuse through porous constructs,[11] and lithium within the crystal diffuses between the surface and the center.[12] Meanwhile, charge-transfer reactions occur at the surface of the electrode material and electrolyte.[13] Any of the

processes may be the performance limiting step depending on chemistry, mode of operation, and design. Accordingly, understanding the detailed mechanism and the impedance of every process is key to improve the design of batteries.

Physics-based mathematical models play an important role in data analysis. Newman et al.[14,15] developed an approach to couple the electrode and crystal scales. Such models have been used to answer questions that are hard to be fully understood by experiment alone. For example, Srinivasan et al.[16] developed a model for a lithium iron-phosphate electrode to understand the sources of energy loss at different power densities. Brady et al.[17] built a model for lithium trivanadate (LiV_3O_8) electrode using method developed by Newman but foregoing the use of a superposition integral formulation on the crystal scale in favor of a more flexible numerical algorithm which allows inclusion of more physics. They obtained the diffusion coefficient of lithium in LiV_3O_8 and determined that transport processes within the crystal appear to be more rapid during charge than discharge.

Compared with other cathode materials, the layered transition-metal oxide $Li(Ni_xMn_yCo_{1-x-y})O_2$ (NMC) is attractive for electric vehicles because of its moderate cost and high energy density.[18,19] As Figs. 1a, 1b shows, an NMC cathode has a hierarchical structure. The ~400 nm primary NMC crystals tends to form spherical agglomerates with an average diameter of ~10 μm. Yang et al.[20] used focused ion beam (FIB) to lift out NMC crystals and used EDS to observe the chemical constitutions on the crystal surfaces. The strong phosphorus signal on the grain boundary conclusively showed that the electrolyte penetrates into the inside of agglomerated crystals and the Li oxidation/reduction reaction occurs at the surface of each of the small crystals instead of at the outer edge of the agglomerate.

In addition to transport across the bulk electrode (electrode scale), there are two length-scales that may impact the transport process: the transport of lithium ion (Li^+) throughout the agglomerate (agglomerate scale), and the diffusion of Li inside NMC crystal (crystal scale). Commonly, researchers in modeling couple the electrode scale to either the agglomerate or crystal scales, but it may be difficult to know which length scale to use. If a diffusion coefficient is independently known, the characteristic times associated with potential relaxation may prove insightful.[21] Often the diffusion coefficient is not known with certainty. Furthermore, agglomerate-scale transport processes have important characteristics that are not always captured with a crystal-scale model, especially at high rates. This may not always be accounted for, and this can impact conclusions as discussed here. Since the characteristic length of the two scales may be vastly different, interpretation of relaxation times in GITT experiments may lead to a very large variation in literature-reported diffusion coefficients.

To determine the more important transport process, this paper compares both electrode-agglomerate scales coupled mathematical model (agglomerate model) and electrode-crystal scales coupled model (crystal model) to experimental results. As Fig. 1c shows, in both models, the assumption is made that the transport process on the other scale is fast enough and the resulting impedance is negligible. Both models are compared under multiple current rates, and model-selection algorithms are used to identify the most important length scale in an electrode construct, at least from the point of view of transport limitations. In other words, the efficacy of models derived from hypothesizing crystal-scale transport limitations are controlling are compared to models derived from hypothesizing agglomerate-scale transport limitations are controlling.

Theory

Mathematical model.—Figure 2a shows the configuration of the coin cell used in this study. Based on such configuration, two models were developed following the development by Knehr[22] et al. and Brady et al.[23] In order to eliminate electrode-scale transport limitations, thin $LiNi_{0.33}Mn_{0.33}Co_{0.33}O_2$($NMC_{111}$) cathodes (25 μm, mass loading = 2.84 mg cm^{-2}) were used in the experimental study and in the present analysis. Both scaling arguments and simulations confirmed that electrode-scale effects were negligible.

Nevertheless, a so-called pseudo 2D modeling paradigm[24] was used to most easily connect the smaller-length scale simulations to the parameters that are controlled during fabrication. Equations describing transport of lithium inside the NMC agglomerate or crystal are coupled to the electrode scale equations. As shown in Fig. 1c, in the crystal model, we assume that the transport through agglomerates is fast and do not contribute to voltage loss, thus the agglomerate scale transport loss is neglected. In contrast, crystal scale transport loss is neglected in the agglomerate model. All the coupled equations are solved simultaneously using the BAND(J) algorithms,[25] which gives values of dependent variables as a function of position and time. Detailed governing equations and boundary conditions are shown in Table I. The coefficients for the reversible potential in Table I, Eq. 11 were obtained by fitting the expression to experimental GITT (C/10) data taken after one hour of relaxation at 11 different state of discharge. While both models describe similar physics, there are differences. For example, the description of the interfacial reaction kinetics appears as a boundary condition in a crystal-scale model but in the governing equation of an agglomerate-scale model.
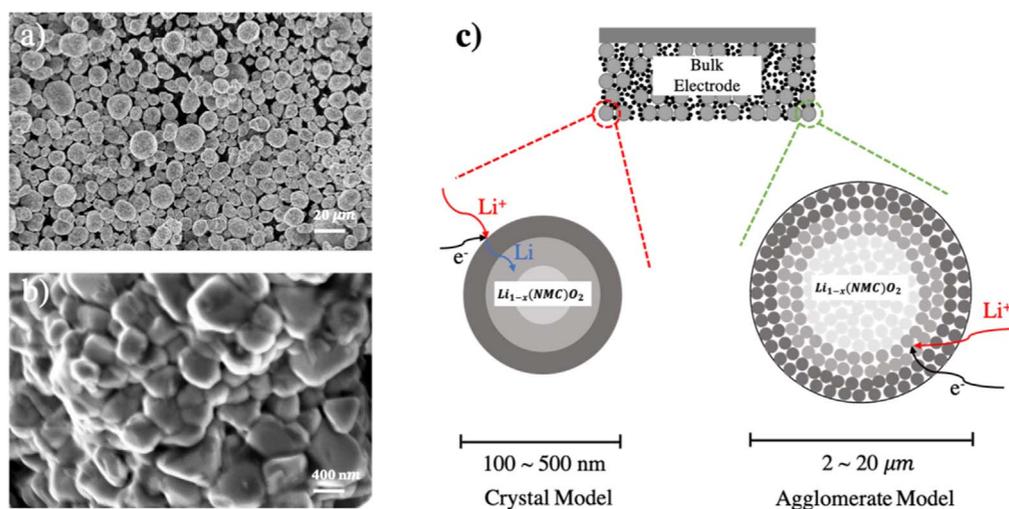

Figure 1. (a) (b) SEM images of *NMC*$_{111}$; (c) Schematic of the assumptions of crystal model and agglomerate model, in which the limiting transport process occurs on the crystal and agglomerate length scales separately.
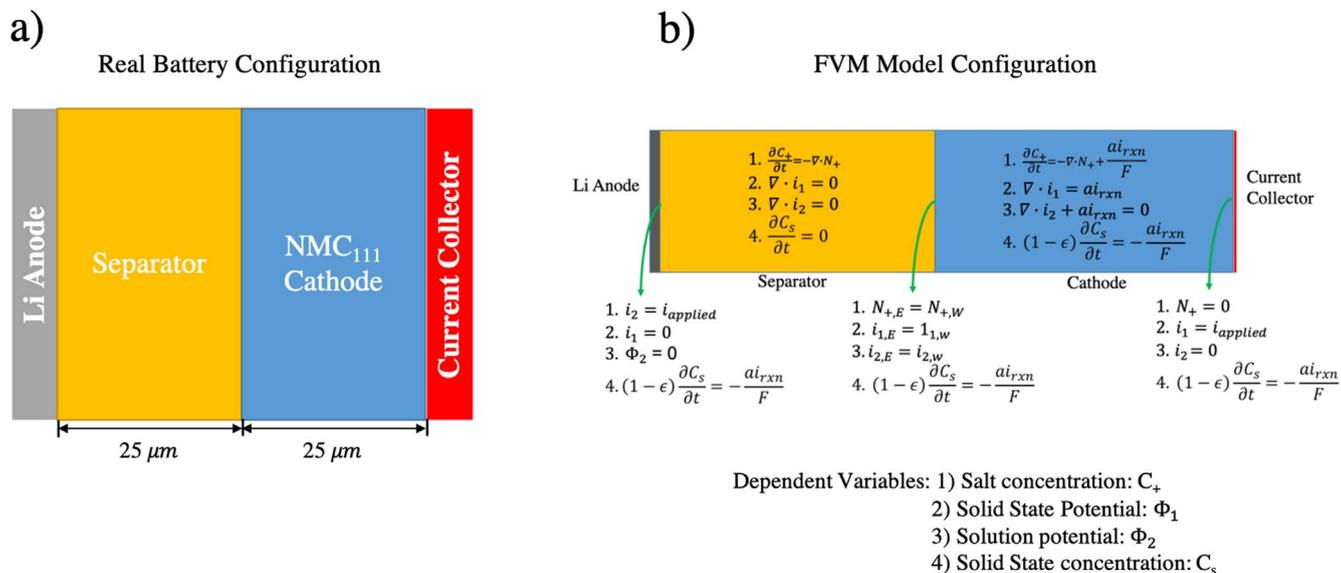
Figure 2. (a) Configuration of real battery. (b) Configuration of physical based continuum model, with electrode scale governing equations and boundary conditions.

Parameter estimation.—The parameter estimation method follows the development of Brady et al.[26] A designated parameter space was sampled using Sobol sequences from Python module sobol_seq.[27] After simulations are generated using different sets of parameters from sobol sampling, the residual sum of squares (RSS) is calculated to describe how well the simulations emulate the experimental data. The RSS value of each parameter set is then fed into a Markov-chain monte-carlo (MCMC)[28] method to show statistical distributions of parameters. The parameter values are assumed to form a normal distribution, in which the mean value is the most likely parameter to emulate real electrochemical performance, and the standard deviation indicates the uncertainty in this parameter estimation.

In our study, a three-parameter space comprised of either the agglomerate or crystal scale diffusion coefficient (D_{agg} or D_x), reaction rate constant k_{rxn} of lithium intercalation inside NMC materials and contact resistance (R_{ct}) is sampled. The assumption that anode impedances can be neglected was tested to confirm the modeling approach. Results indicate that the anode overpotential is on the order of 1–2 mV for 0.85 mA cm^{-2} (2C) discharge. It was concluded that the estimation of the agglomerate-scale diffusion coefficient is not impacted by inclusion of the anode overpotential.

Experimental

Cathode casting.—Cathodes were cast on ∼18 μm Al foil with doctor blades using a mixture of $LiNi_{0.33}Mn_{0.33}Co_{0.33}O_2$ (MSE Supplies LLC), carbon black (Timcal), and PVDF (Arkema Kynar 761) at a mass ratio of 9:0.5:0.5, dissolved in N-Methyl-2-Pyrrolidone (NMP) (Sigma-Aldrich). The as-casted electrode was heated on a hot plate to 110 °C to evaporate NMP solvent and cathode with mass loading ∼2.84 mg cm^{-2} could be obtained. Such 25 μm NMC_{111} cathode contains NMC agglomerates with average diameter of 10 μm and NMC crystals with an average diameter of 400 nm.

Coin cell assembling.—CR2032 Coin cells were made inside an argon filled glovebox. A commercial electrolyte, 1 M $LiPF_6$ in EC/DEC (5:5, w/w) (Gotion Inc.) was used as liquid electrolyte. 250 μm lithium metal foils were used as counter electrode. After assembly, two formation cycles at a C/10 rate were conducted prior to the galvanostatic and GITT experiments, which were performed employing a Landt battery tester.

Results

Select cathode thickness to eliminate electrode scale transport effect.—Mass transport processes occur at a minimum of at least three different length scales inside the NMC electrode: electrode scale, agglomerate scale and crystal scale. In order to characterize the agglomerate scale and crystal scale mass transport, it is helpful to design experiments in which variations on the electrodes scale are negligible. Intuitively, this implies the use of thin electrodes, and Brady et al.[26] showed that mock experiments can quantitively show when a parameter is not important. Specifically, in this case, when the simulated uncertainty σ_{D_0} of the electrode-scale effective diffusion coefficient is large and $\sigma_{D_{agg}}$ is small, the electrode scale is not important. Figure 3 shows the normalized parameter estimation results for cathodes with different thickness (mock experiments). Comparing the uncertainty of electrode scale diffusion coefficient (σ_{D_0}) and agglomerate scale diffusion coefficient ($\sigma_{D_{agg}}$), the result suggests that for thick cathodes (>100 μm), the electrode scale mass transport is more important. While for thin electrodes, the electrode scale transport impedance is negligible. Thus, as we want to eliminate the electrode effect, a thin cathode (25 μm) was used to obtain experimental data for further study.

Testing hypotheses by comparing models to galvanostatic experimental data.—To compare the simulation results derived from the two alternative hypotheses, the agglomerate model and crystal model were trained using galvanostatic experiments. The cell was operated between 3.0 V and 4.3 V under 0.2 C, 0.33 C, 0.5 C, 1 C and 2 C, in which 1 C = 150 mA g^{-1}. For model training, models were fitted to discharge voltage profiles under the 5 current rates, and a single set of parameters was obtained. For the agglomerate model, the diffusion coefficient $D_{agg} = (1.2 \pm 0.2) \times 10^{-9}$ cm^2 s^{-1}, which is within a reasonable range compared with others' reports.[29,30] This low diffusion coefficient might result from the close packing of NMC crystals inside the agglomerate, which can be observed in Fig. 1b. For the crystal scale model, a value of $D_x = (5.2 \pm 2.6) \times 10^{-12}$ cm^2 s^{-1} is obtained. The diffusion coefficient obtained from a crystal scale model is characterized by a significantly higher uncertainty. The higher uncertainty is because the parameter estimation algorithm suggests that the transport impedance is less dominant in the crystal-scale model.

Figure 4 shows the experimental voltage profiles and simulation results for both models. Simulation results do not extend to the

Table I. Governing equations and boundary conditions for mathematical model of NMC cell.

Electrode Scale Equation

	Governing Equation	Li Anode	Separator Edge	Current Collector
(1) Solid State Current (i_1)	$(1-\epsilon)\sigma\nabla^2\Phi_1 - ai_{in} = 0$	$i_1 = 0$	$\nabla \cdot i_1 = 0$	$i_1 = i_{applied}$
(2) Electrolyte Current (i_2)	$\nabla \cdot (\kappa\nabla\Phi_2) + \epsilon F(z_+D_+ + z_-D_-)\nabla^2 c_0 + ai_{in} = 0$ $(\kappa = \epsilon F^2(z_+^2 u_+ + z_-^2 u_-)c_0)$	$\Phi_2 = 0$	$\nabla \cdot i_2 = 0$	$i_2 = 0$
(3) Electrolyte Concentration (c_0)	$\epsilon\frac{\partial c_0}{\partial t} = -\nabla \cdot N_+ + \frac{ai_{in}}{F}$ $\left(N_+ = -D_{0,eff}\nabla c_0 - \frac{F}{RT}z_+D_+c_0\nabla\Phi_2\right)$	$N_+ = \frac{i_{applied}}{F}$	$\nabla \cdot N_+ = 0$	$N_+ = 0$
(4) Solid State Concentration (c_s)	$(1-\epsilon)\frac{\partial c_s}{\partial t} = -\frac{a\cdot i_{in}}{F}$	—	—	—

Crystal Scale equation

	Governing equation	Crystal Center	Crystal Edge
(5) Lithium balance ($c_s{}^x$)	$\frac{\partial c_s{}^x}{\partial t} = D_x\nabla^2 c_s{}^x$	$\nabla c_s{}^x = 0$	$-D_x\nabla c_s{}^x = \frac{i_{in}}{F}$

Agglomerate Scale equation

	Governing equation	Agglomerate Center	Agglomerate Edge
(6) Solid State Current (i_1^{agg})	$\nabla \cdot i_1^{agg} = a^{agg}i_{in}^{agg}$ $\left(i_{surface,agg} = \frac{\partial C_s}{\partial t}FV_{agg}(1-\epsilon_{agg})/A_{agg}\right)$	$i_1^{agg} = 0$	$i_1^{agg} = i_{surface,agg}$
(7) Electrolyte Current (i_2^{agg})	$\nabla \cdot i_2^{agg} = a^{agg}i_{in}^{agg}$	$i_2^{agg} = 0$	$\Phi_2^{agg} = \Phi_2$
(8) Electrolyte Concentration (c_0^{agg})	$\epsilon^{agg}\frac{\partial c_0^{agg}}{\partial t} = -\nabla \cdot N_+^{agg} + \frac{a^{agg}i_{in}^{agg}}{F}$ $\left(N_+^{agg} = -\epsilon^{agg}D_{agg}\nabla c_0^{agg} - \frac{F}{RT}z_+D_{agg}c_0^{agg}\nabla\Phi_2^{agg}\right)$	$N_+^{agg} = 0$	$c_+^{agg} = c_{bulk}$
(9) Solid State Concentration (c_s^{agg})	$(1-\epsilon^{agg})\frac{\partial c_s^{agg}}{\partial t} = -\frac{a^{agg}i_{in}^{agg}}{F}$	—	—

Electrochemical Reaction Rate

(10) Current Density (i_{in})	$i_{in} = i_0\left[\exp\left(\frac{\alpha_a F\eta}{RT}\right) - \exp\left(-\frac{\alpha_c F\eta}{RT}\right)\right]$	$\eta = \Phi_1 - \Phi_2 - U$
Exchange Current Density (i_0)	$i_0 = Fk_{rxn}c_0^{\alpha_a}c_\alpha^{\alpha_c}(c_{\alpha,\,max} - c_\alpha)^{\alpha_a}$	

Reversible Potential

$$(11) \quad U = U_{ref} + \frac{RT}{F}\ln\left[\left(\frac{c}{c_0}\right)\left(\frac{1-\bar{c}_{max}}{\bar{c}_{max}}\right)\right] + \sum_{k=0}^{10} A_k\left[(2\bar{c}_{max}-1)^{k+1} - \frac{2\bar{c}_{max}k(1-\bar{c}_{max})}{(2\bar{c}_{max}-1)^{1-k}}\right]$$

$$\bar{c}_{max} = \frac{c_s - c_{s,0}}{c_{s,\,max} - c_{s,0}}$$

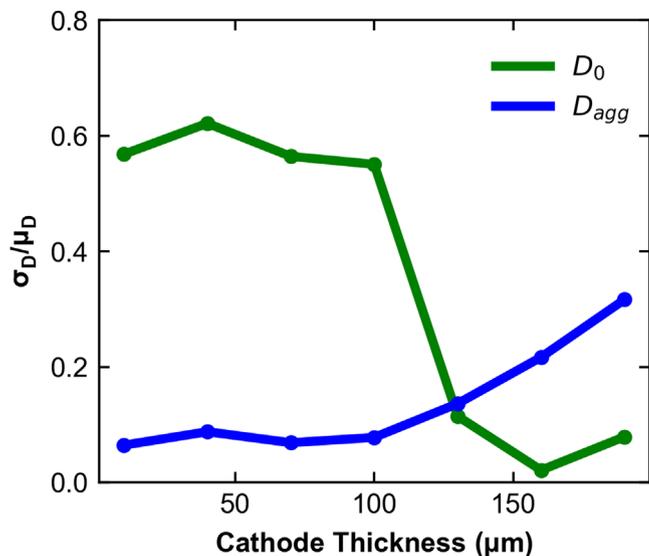| Parameter	Value	Parameter	Value	Parameter	Value
$c_{s,\,max}$ (mol cm^{-3})	0.0262	A_3	0.023162	A_8	−0.259945
U_{ref} (V)	3.868568	A_4	−0.037789	A_9	−0.589845
A_0	−0.201805	A_5	−0.330780	A_{10}	0.052014
A_1	0.112340	A_6	0.239297		
A_2	−0.048369	A_7	0.778712		

Figure 3. Parameter estimation results (normalized uncertainty: σ_D/μ_D) for electrode scale diffusion coefficient (D_0) and agglomerate scale diffusion coefficient (D_{agg}) at different cathode thickness.
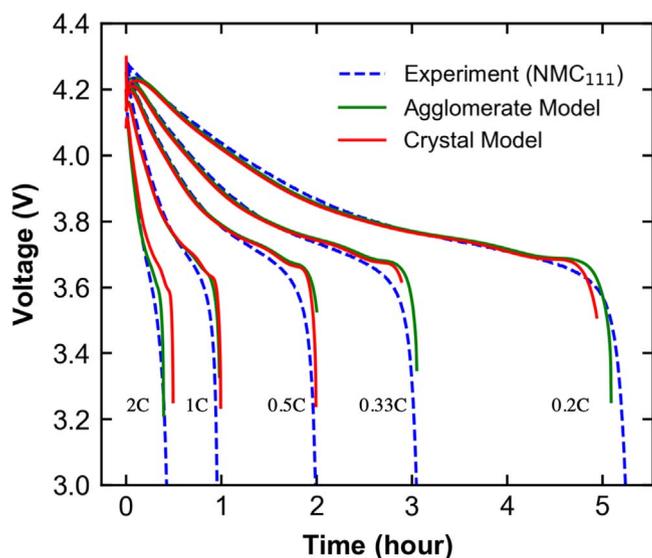

Figure 4. Comparison of experimental galvanostatic discharge voltage profile to agglomerate model & crystal model simulation results.

experimental cutoff (2.8 V) because of numerical limitations. Both models agree with experimental data for C-rates below 1 C. For the 2 C rate, the agglomerate model still agrees well with experimental performance, while the crystal model is less successful at the large depth of discharge.

Check consistency of parameter values from different training sets.—Another method for model selection or hypothesis testing is to compare parameter estimates of the two models when trained with different types of experiments. Ideally, the derived parameters are consistent. Here, models were trained by (1) galvanostatic discharge experiments and (2) relaxation (voltage recovery) experiments. Figure 5 show the probability distribution function for the diffusion coefficient obtained by the two models when trained with discharge data and relaxation data. The experimental variation (s_{exp}) is estimated to be 20 mV. It can be seen that for the agglomerate model, discharge and relaxation experiments yield very similar estimates. This is seen in Fig. 5c, where $D_{discharge}/D_{relaxation} = 0.85 \pm 0.2$. In contrast, the mean crystal-

scale state diffusion coefficient (D_x) estimated from discharge and relaxation is 5.2×10^{-12} cm^2 s^{-1} and 1.7×10^{-12} cm^2 s^{-1}. In Fig. 5c, we see $D_{discharge}/D_{relaxation} = 3.1 \pm 1.7$ for the crystal model.

For an ideal system with experimental measurements with no variance, the ratio of diffusion coefficients should be one. In our case, for the agglomerate model, the distribution of $D_{discharge}/D_{relaxation}$ is narrow and has a mean value relatively close to 1. To be more quantitative, the agglomerate model has a 97% chance that $D_{discharge}/D_{relaxation}$ is between 0.6 and 1.4. For the crystal model, there is only a 17% chance that the ratio falls in this range. Thus, by comparing parameter values from different experimental sets for model selection, the agglomerate model has a much higher probability to be correct.

Comparing prediction error.—Another means of model selection is to evaluate its prediction ability. Similar to leave-one-out cross validation,[31] the model is trained on a combination of data sets to obtain parameters. Then the trained model is used to predict the experimental performance of a test set that is not included in the training sets. In this study, the training sets and test sets were selected from 0.1C, 0.2C, 0.33C, 0.5C, 1C and 2C discharge experiments. To start, the models were trained by the lowest rate (0.1C) to predict the performance at 0.2C. Then the models were trained using a combination of 0.1C and 0.2C to predict 0.33C performance. For the last step, all other current rates was used to predict the performance of 2C discharge. This is named "forward prediction." For "backward prediction," The models are trained by 2C to predict 1C, etc. Figure 6 shows the average prediction error, which is the average deviation of prediction from experimental data (e_{sim}) normalized by the experimental variation ($s_{exp} = 20$ mV):

$$\bar{e}_{sim} = \frac{e_{sim}}{s_{exp}} \qquad [1]$$

For both forward and backward prediction, the prediction errors are similar for C-rates less than 0.5C. However, the error starts to differentiate at the higher discharge rates. For 1C prediction, the backward method for the crystal model has a high normalized error ($\bar{e}_{sim} \sim 3$), while the error for the agglomerate model is relatively low ($\bar{e}_{sim} \sim 1.2$). For 2C prediction, the forward prediction by the agglomerate model has much lower error than crystal model. This further suggests that the agglomerate scale model is in better agreement with experiment than the crystal-scale model. The deviation at 2C is also seen in Fig. 4, but perhaps in a less convincing manner.

Comparing models to experimental dV/dQ profiles.—In some cases, it may be desirable to predict the changes in voltage rather than the voltage, especially when an experimental uncertainty (such as a contact resistance or anode impedance in a cathode study) is difficult to eliminate. In such cases, models can be trained on for example a dV/dQ curve, which is the derivative of the voltage with respect to discharge capacity. The two models were trained using dV/dQ profiles for 0.33C, 0.5C, 1C and 2C and the resulted simulation results are shown in Fig. 7. Just as in Fig. 3, by fitting to dV/dQ curve, the two models are only distinct at 2C. The agglomerate model agrees better with experimental dV/dQ. Results gave $D_{agg} = (1.2 \pm 0.2) \times 10^{-9}$ cm^2 s^{-1}, identical to values obtained by fitting V vs time. For the crystal scale model, $D_x = (5.9 \pm 2.5) \times 10^{-12}$ cm^2 s^{-1}, which are also close to values obtained by fitting V vs time.

Diffusion coefficient as a function of state of charge (SOC).—Often, experimental investigations are not closely integrated with modeling development. Thus, a broadly applied theory is often used to estimate diffusion coefficient[32,33]:
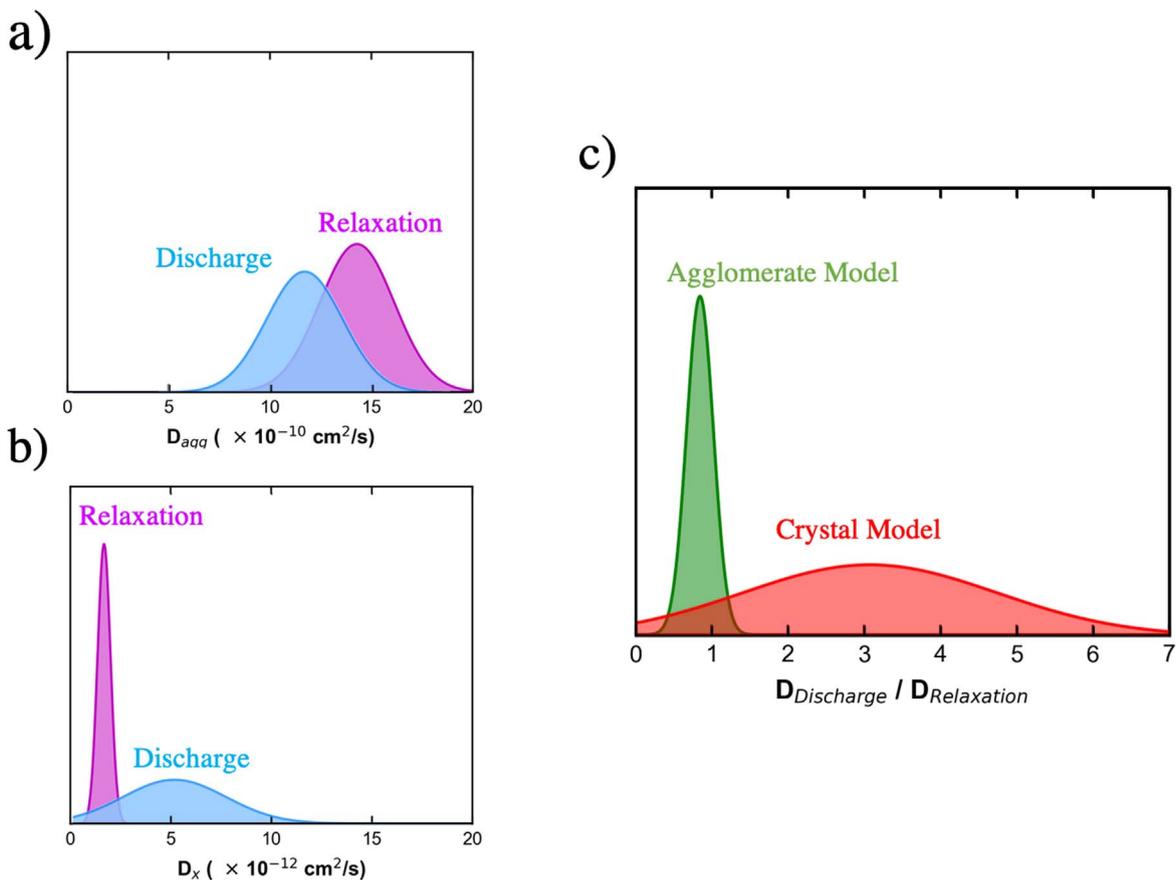
Figure 5. (a) and (b) Probability distribution functions of D_{agg} in the agglomerate model and D_x in the crystal model by fitting to discharge data and relaxation data respectively. (c) Distribution of $D_{discharge}/D_{relaxation}$ for agglomerate model and crystal model.
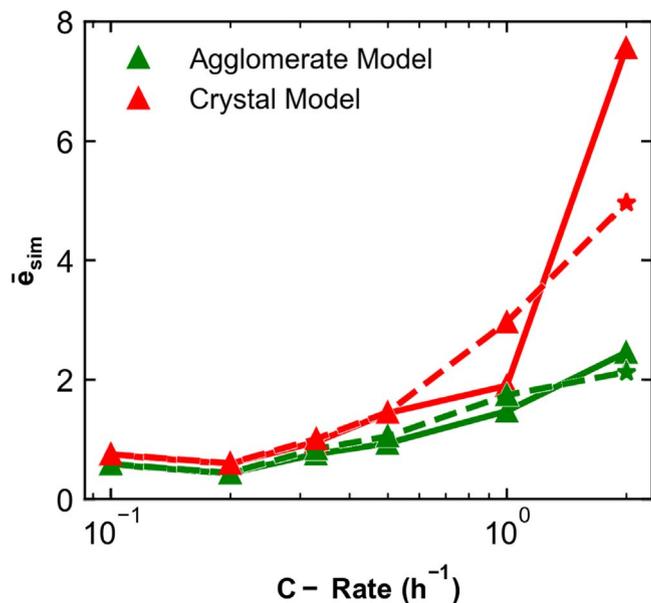

Figure 6. Prediction error for "forward prediction" (solid lines) and "backward prediction" (dashed lines). The stars are the initial fitted model errors (0.1C for "forward prediction" and 2C for "backward prediction") emanating from the initial parameter estimates used for predictions.

$$\tilde{D} = \frac{4}{\pi\tau}\left(\frac{m_B V_M}{M_B S}\right)^2 \left(\frac{\Delta E_s}{\Delta E_t}\right)^2 \quad (\tau \ll L^2/\tilde{D}) \qquad [2]$$

where $\tau(s)$ is the time duration for each discharge step, $m_B(g)$ is the mass of NMC, M_B (g mol^{-1}) is the atomic weight of NMC, V_M (cm^3 mol^{-1}) is the molar volume of the NMC materials, S (cm^2) is the area of electrode. $\Delta E_s(V)$ and $\Delta E_t(V)$ are the change of voltage between relaxations and during discharge.

Note that Eq. 2 is derived assuming a crystal scale model, and the inequality constraint arises because the physics used to derive Eq. 2 assumes semi-infinite diffusion.[34] The use of Eq. 2 may lead to, for example, a conclusion that the diffusion coefficient is a function of the state of charge (SOC). While that is theoretically possible if not probable, whether it leads to improved agreement with experiment is a valid question.

To study the apparent SOC dependency of the diffusion coefficient, voltage recovery data from GITT experiments are used to determine the diffusion coefficient values from the two models, with results shown in Table II. Instead of absolute diffusion coefficients, values of D/L^2 are shown, where L is the diffusion length. Also, D/L^2 values calculated from experimental GITT data by Eq. 2 are listed. Figure 8 shows D/L^2 from agglomerate model fitting, crystal model fitting and from Eq. 2 calculation at 1C.

As shown in Table II and Fig. 8, for the agglomerate model, the D/L^2 value is relatively constant with state of charge. In short, a constant diffusion-coefficient model is consistent with experiment. The crystal scale model suggests that D_x increases with state of charge (this corresponds to decreasing D_x with increasing solid-state Li concentrations). Note however, that the value of D_x remains inconsistent with values estimated from the discharge curve (cf.,
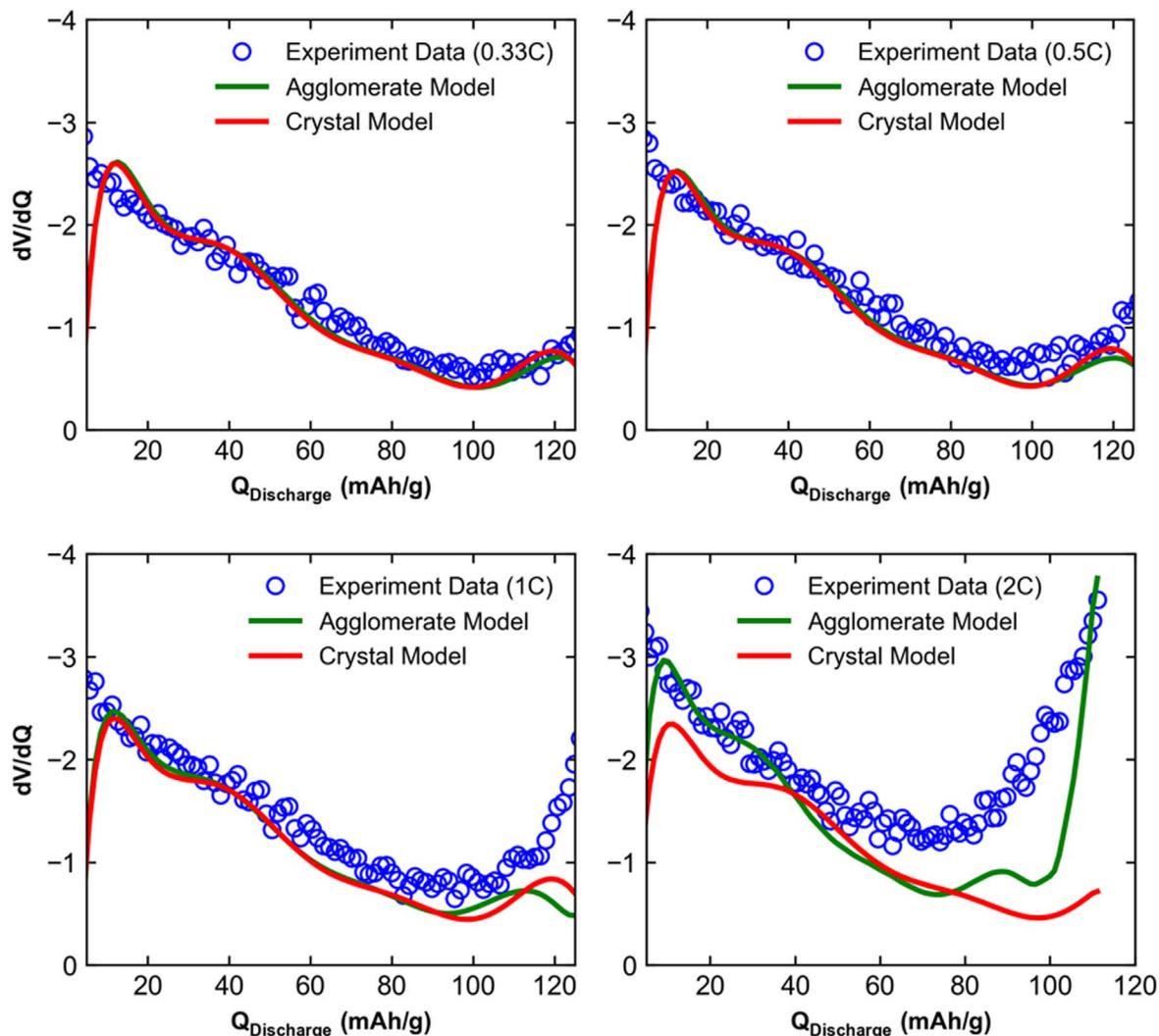
Figure 7. Comparison of experimental galvanostatic discharge dV/dQ profile to agglomerate model & crystal model.

Table II. D/L^2 **values from fitting agglomerate model (Agg) and crystal model (Xtal) to relaxation experiments at different SOC, and** D/L^2 **values calculated by Eq. 2.**

SOC	C/2			1C			2C		
	Equation 2	Agg	Xtal	Equation 2	Agg	Xtal	Equation 2	Agg	Xtal
83.3%	0.97	6.97	3.94						
80%				1.56	4.70	4.72			
66.7%	0.88	5.82	2.27				1.68	6.17	3.68
60%				1.42	4.69	3.32			
50%	0.77	7.03	1.64						
40%				1.08	4.67	1.96			
33.3%	0.4	6.16	0.87				0.55	5.33	2.06
20%				0.42	4.47	1.96			
μ	0.76	6.50	2.17	1.12	4.63	2.99	1.12	5.75	2.87
σ	0.22	0.52	1.13	0.44	0.09	1.14	0.56	0.42	0.81

Fig. 4). Furthermore, diffusion coefficients fit through agglomerate and crystal models are consistent with values obtained by Eq. 2 only to an order of magnitude.

Discussion

The two models are hard to distinguish at relatively low discharge rates (lower than 1C in this paper), without simultaneously considering GITT relaxation data. This was unexpected based on previous experience.[22] Design of experimental conditions that allow for a distinction between the two models is possible. In this experimental design, the diffusion coefficient is assumed to be known. Thus, the problem explores whether an crystal model, which is fitted to agglomerate model simulations, can predict agglomerate models results under new conditions. If it can, then the models are indistinguishable.
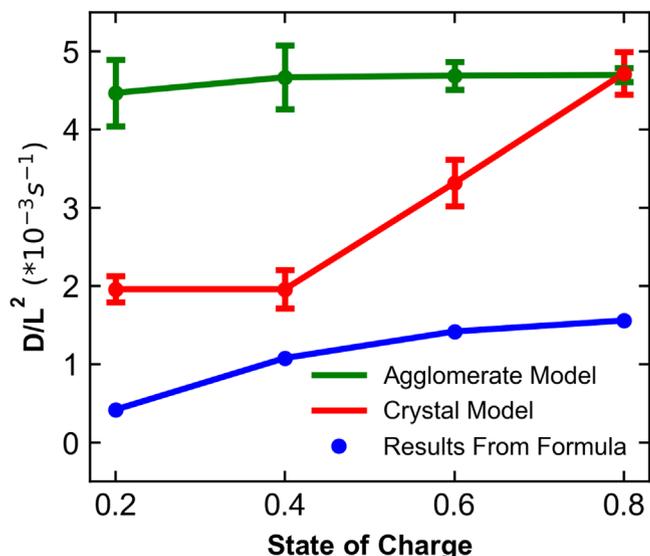
Figure 8. D/L^2 values for agglomerate model (Agg), crystal model (Xtal) and Eq. 1 at 1C rate experiment.

The algorithm works the same as the prediction test of Fig. 6, except it is now applied to mock data. For example, the agglomerate model is fitted to low C-rate crystal model results, and then used to predict performance at higher rates. The resulting error (red curve) is shown in Fig. 9a. At high C-rates, the models are distinguishable as evidenced by the growing error. The reverse is also shown, where the green curve corresponds to applying the crystal model to agglomerate model results. In both cases, the errors grow after 1C, indicating that the 1C rate is the critical current rate in this system. ***In other words, for current rates above 1C, the two models perform differently.***

In contrast to the NMC cathode, when Knehr[22] et al. applied model selection to multi-scale magnetite cathodes, crystal and agglomerate models were distinguishable at all tested C-rates. This indicates that the critical current rate is dependent on the intrinsic properties of the materials studied. To explore further, mock experiments were generated using the agglomerate model, with smaller D_{agg}. As shown in Fig. 9b, the critical current rate to distinguish between two models is 0.1C. In an attempt to generalize this problem, a dimensionless C-rate given by

$$\bar{C}_{rate} \cdot = C_{rate} \cdot \frac{L_{agg}}{D_{agg}} \cdot L_x \qquad [3]$$

where L_{agg} is the mean radius of the agglomerate and L_x is the mean radius of the crystal, was introduced.

Figure 10a shows the prediction error with different materials properties (applied on agglomerate "Mock Data"). The absolute critical current rate is dependent on D_{agg}, L_{agg} and L_x. When using dimensionless current rate ($\bar{C}_{rate}$), the errors start to increase near $\bar{C}_{rate} \sim 10^{-2}$, as shown in Fig. 10b. Due to the complexity of the multiscale model, in which modeling details are chemistry specific, we did not attempt further analyses to collapse the error to a single curve. The black star in Fig. 10b shows the dimensionless current rate of magnetite calculated using parameters from the study by Knehr[22] et al. The value of $\bar{C}_{rate}$ for C/200 was greater than 0.1 for magnetite, explaining why the models were easily distinguishable even at very low C-rates. This result indicates that the critical current rate to distinguish between agglomerate and crystal model depends on size of agglomerate (L_{agg}), the size of crystal (L_x) and the diffusion coefficient on one of the two smaller scales (D_{agg} here).

Conclusions

Model selection approaches can be used to determine whether an agglomerate-scale or crystal-scale model is more consistent with experiment. Under some experimental conditions, the models are indistinguishable. Model-guided design of experiments can be used to most conclusively test competing hypotheses. At low C-rates, crystal scale and agglomerate scale models are indistinguishable if the diffusion coefficient is assumed to be an unknown fit to experiment. For NMC_{111} material, agglomerate scale diffusion, which is the diffusion of lithium across the secondary particles was determined to be rate limiting. This conclusion is supported by multiple algorithmic approaches that test consistency between experiments and the prediction efficacy of the models.
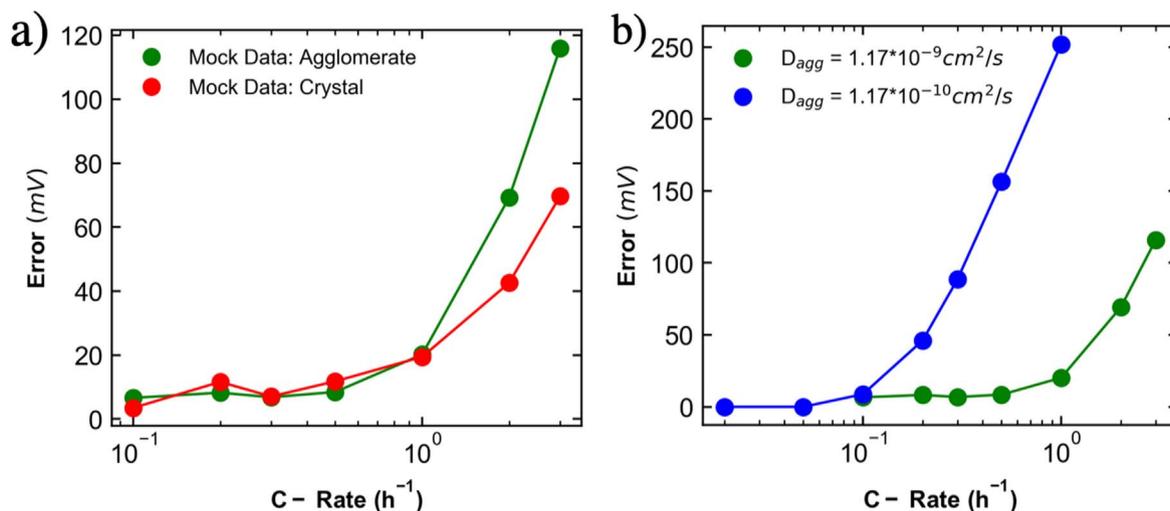
Figure 9. (a) Prediction error as a function of current rate, using agglomerate model (green) and crystal model (red) to generate "Mock experiments," respectively. (b) Prediction error when using agglomerate model with different D_{agg} to generate "Mock experiment."
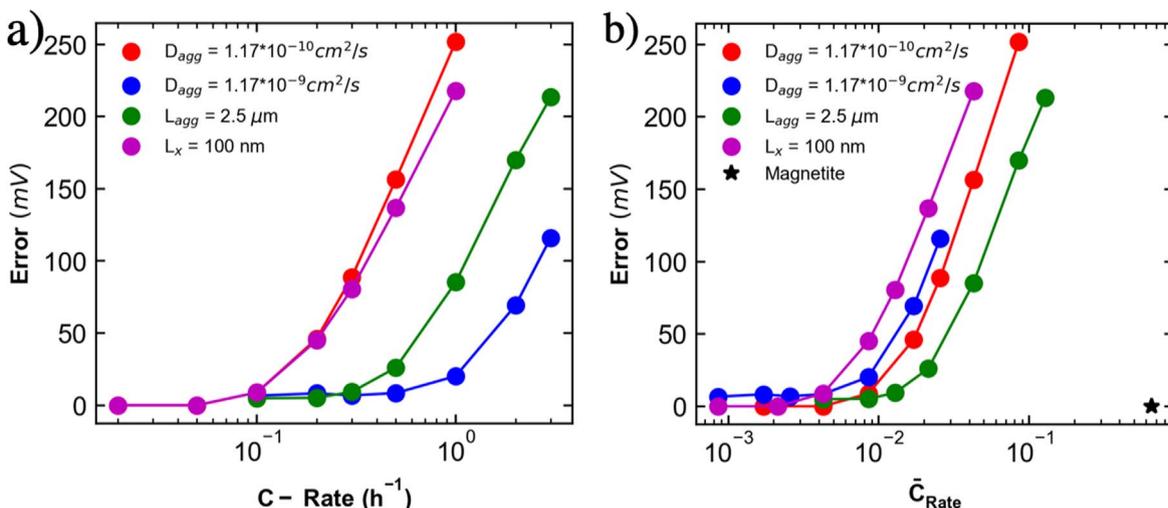
Figure 10. (a) Prediction Error as a function of absolute current rate, "Mock experiments" generated by agglomerate model with different material parameters. (b) Prediction Error as a function of dimensionless current rate. For red "Mock experiments," $D_{agg} = 1.17 \times 10^{-10}$ cm^2, $L_{agg} = 5\,\mu$m and $L_x = 200$ nm. Each of other "Mock experiments" have one parameter with different value. For magnetite, only dimensionless current rate is shown here to compare with NMC cathode in this study.

ORCID

Alan C. West ⓘ https://orcid.org/0000-0002-3524-3040

References

1. M. S. Whittingham, *Chem. Rev.*, **114**, 11414 (2014).
2. G. E. Blomgren, *J. Electrochem. Soc.*, **164**, A5019 (2017).
3. V. Etacheri, R. Marom, R. Elazari, G. Salitra, and D. Aurbach, *Energy & Environmental Science*, **4**, 3243 (2011).
4. L. Lu, X. Han, J. Li, J. Hua, and M. Ouyang, *J. Power Sources*, **226**, 272 (2013).
5. J. Liu et al., *Nat. Energy*, **4**, 180 (2019).
6. S. Chen, C. Niu, H. Lee, Q. Li, L. Yu, W. Xu, J.-G. Zhang, E. J. Dufek, M. S. Whittingham, and S. Meng, *Joule*, **3**, 1094 (2019).
7. R. Marom, S. F. Amalraj, N. Leifer, D. Jacob, and D. Aurbach, *J. Mater. Chem.*, **21**, 9938 (2011).
8. M. Singh, J. Kaiser, and H. Hahn, *J. Electrochem. Soc.*, **162**, A1196 (2015).
9. M. Hu, X. Pang, and Z. Zhou, *J. Power Sources*, **237**, 229 (2013).
10. M. D. Radin, S. Hy, M. Sina, C. Fang, H. Liu, J. Vinckeviciute, M. Zhang, M. S. Whittingham, Y. S. Meng, and A. Van der Ven, *Adv. Energy Mater.*, **7**, 1602888 (2017).
11. L. O. Valøen and J. N. Reimers, *J. Electrochem. Soc.*, **152**, A882 (2005).
12. E. Antolini, *Solid State Ionics*, **170**, 159 (2004).
13. C. Julien, *Materials Science and Engineering: R: Reports*, **40**, 47 (2003).
14. M. Doyle, T. F. Fuller, and J. Newman, *J. Electrochem. Soc.*, **140**, 1526 (1993).
15. T. F. Fuller, M. Doyle, and J. Newman, *J. Electrochem. Soc.*, **141**, 1 (1994).
16. V. Srinivasan and J. Newman, *J. Electrochem. Soc.*, **151**, A1517 (2004).
17. N. W. Brady, Q. Zhang, K. Knehr, P. Liu, A. C. Marschilok, K. J. Takeuchi, E. S. Takeuchi, and A. C. West, *J. Electrochem. Soc.*, **163**, A2890 (2016).
18. N. Yabuuchi and T. Ohzuku, *J. Power Sources*, **119**, 171 (2003).
19. X. Y. Zhang, W. J. Jiang, A. Mauger, Qilu, F. Gendron, and C. M. Julien, *J. Power Sources*, **195**, 1292 (2010).
20. P. F. Yang, J. M. Zheng, S. Kuppan, Q. Y. Li, D. P. Lv, J. Xiao, G. Y. Chen, J. G. Zhang, and C. M. Wang, *Chem. Mater.*, **27**, 7447 (2015).
21. W. Weppner and R. A. Huggins, *J. Electrochem. Soc.*, **124**, 1569 (1977).
22. K. W. Knehr, N. W. Brady, C. A. Cama, D. C. Bock, Z. Lin, C. N. Lininger, A. C. Marschilok, K. J. Takeuchi, E. S. Takeuchi, and A. C. West, *J. Electrochem. Soc.*, **162**, A2817 (2015).
23. N. W. Brady, Q. Zhang, A. Bruck, D. C. Bock, C. A. Gould, A. C. Marschilok, K. Takeuchi, E. Takeuchi, and A. C. West, *J. Electrochem. Soc.*, **165**, A371 (2018).
24. B. Paxton, *J. Electrochem. Soc.*, **144**, 3818 (1997).
25. J. Newman and E. Thomas-Alyea, *Electrochemical Systems* (John Wiley & Sons, New York) (2004).
26. N. W. Brady, C. A. Gould, and A. C. West, *J. Electrochem. Soc.*, **167**, 013501 (2020).
27. H. Niederreiter, *J. Number Theory*, **30**, 51 (1988).
28. W. K. Hastings, *Biometrika*, **57**, 97 (1970).
29. R. Amin and M. Chiang, *J. Electrochem. Soc.*, **163**, A1512 (2016).
30. Z.-D. Huang, X.-M. Liu, S.-W. Oh, B. Zhang, P.-C. Ma, and J.-K. Kim, *J. Mater. Chem.*, **21**, 10777 (2011).
31. A. M. Molinaro, R. Simon, and R. M. Pfeiffer, *Bioinformatics*, **21**, 3301 (2005).
32. R. Amin and Y. M. Chiang, *J. Electrochem. Soc.*, **163**, X7 (2016).
33. S. Cui, Y. Wei, T. Liu, W. Deng, Z. Hu, Y. Su, H. Li, M. Li, H. Guo, and Y. Duan, *Adv. Energy Mater.*, **6**, 1501309 (2016).
34. W. Weppner and R. A. Huggins, *J. Electrochem. Soc.*, **124**, C135 (1977).